An experimental investigation of a solar-driven desalination system based on multi-effect membrane distillation

A. Najib[a], J. Orfi[a], H. Alansary[a], E. Ali[b,*], Z. Abdulwahed[c], S. Alzahrani[b], A. Chafidz[d]

[a]_Mechanical Engineering Department, King Saud University, Riyadh, Saudi Arabia, emails: anmohammed@ksu.edu.sa (A. Najib), orfij@ksu.edu.sa (J. Orfi), hansary@ksu.edu.sa (H. Alansary)_
[b]_Chemical Engineering Department, King Saud University, Riyadh, Saudi Arabia, emails: amkamal@ksu.edu.sa (E. Ali), szahrani@ksu.edu.sa (S. Alzahrani)_
[c]_Sustainable Energy Center Technologies, King Saud University, Riyadh, Saudi Arabia, email: z.haidar1@yahoo.com (Z. Abdulwahed)_
[d]_Chemical Engineering Department, Universitas Islam Indonesia, Yogyakarta, Indonesia, email: achmad.chafidz@uii.ac.id (A. Chafidz)_

ABSTRACT

We investigate the effectiveness of an integrated solar-driven system with a membrane-distillation process for freshwater production. A system is a self-powered unit that comprises a solar-photovoltaic system, solar–thermal system, and membrane-distillation system. A vacuum multi-effect membrane distillation (V-MEMD) module acts as the core of the solar desalination unit, and a heat pump is integrated to the module to improve its performance. We focus on evaluating the overall energy consumption, both thermal and electric, for the cases with and without condenser cooling. The system was tested in Riyadh over two seasons, that is, summers and winters. Upon enabling the preheat mode during June, March, and April, the maximum distillate-water production and the corresponding minimum specific electrical-energy consumption (SEEC) were achieved at approximately 31.8 L/h and 74.9 kWh/m^3, respectively, for the overall system, and the SEEC for the V-MEMD unit also reached 6.3 kWh/m^3. Furthermore, when the inlet heating (evaporator) temperature was greater than 55°C, cold-side absolute pressure was lower than 200 mbar, and preheat mode was active, then high water mass flux up to 12.2 kg/m^2 h and recovery ratio up to 36.8% could be obtained. Moreover, the gain output ratio enhanced to 4.25.

Keywords: Solar thermal desalination; Multi-effect membrane distillation; Recovery ratio; Gain output ratio (GOR); Specific electrical-energy consumption (SEEC); Specific thermal-energy consumption (STEC)

1. Introduction

Nowadays, the demand for freshwater is becoming a critical issue for several countries. Therefore, the development of reliable and efficient systems that contribute to reducing the scarcity of potable water is rapidly increasing. The widely used desalination technology involves reverse osmosis (RO) followed by multi-stage flash distillation (MSF) [1]. These desalination systems consume a significant amount of energy and incur high operating costs. Because of water scarcity in Saudi Arabia, several full-scale desalination plants that operate mainly using fossil fuels were developed [1,2]. For economic and environmental reasons, linking green-energy sources, such as solar-energy, geo-thermal-energy, and waste-energy resources to desalination systems is important. Utilizing renewable energy to operate seawater-desalination processes will alleviate their environmental impact and enhance their sustainability

* Corresponding author.

[3–6]. Notably, solar energy is the most abundant renewable-energy source [7]. It can be used to drive a seawater-desalination process either by generating thermal energy to drive phase-change processes (e.g., multi-effect distillation (MED) and membrane distillation (MD)) or by generating electricity to drive membrane processes (e.g., RO) [8]. Such an approach is considerably appropriate for application in regions that have surplus solar energy but scarce natural-water sources, such as Saudi Arabia and other the Middle East and North African countries.

MD is a promising separation process for purifying saline water. It is a hybrid of the thermally driven desalination process and the membrane-separation process, which is described as trans-membrane evaporation [8,9]. Unlike RO, which relies on total pressure difference, MD separation is based on the transmembrane vapor pressure difference [10,11]. The MD process can be classified into the following four basic configurations: direct-contact MD (DCMD), air-gap MD (AGMD), sweeping-gas MD, and vacuum MD (VMD) [4,12]. In recent years, several studies have been performed on the design, building, and performance tests of small-scale solar MD units. Such units integrate both solar thermal collectors and photovoltaic (PV) panels to feed MD desalination components. An example of such units is the plant situated at the Jordan University of Science and Technology campus for performing tests in the weather of Jordan. The plant production is 120 L/d, and the associated thermal energy consumption lies between 200 and 300 kWh/m³ [8]. Another example is the solar MD system at Alexandria University, Egypt, which couples desalination system with solar thermal collectors and PV [13]. On a sunny day, with 7.25 kWh/d, the results indicate the production of approximately 11.2 L/d for every 1 m² of the solar collector area. Koschikowski et al. [14] experimentally investigated the performance of solar thermally driven compact desalination systems based on MD for the capacity ranging from 100 to 500 L/d. Guillén-Burrieza et al. [15] experimentally investigated the performance of an AGMD system integrated with solar energy by using several indicators such as distillate-water quality, thermal efficiency, and recovery ratio. The maximum specific distillate flux was approximately 7 L/m²h. Bouguecha et al. [16] investigated the performance and thermal-energy efficiency of a DCMD system integrated with solar collectors. The plant included four main loops. The first loop comprised solar collectors with a total area of 20 m². The second loop comprised PV panels, with a peak output of 1.48 kW$_{peak}$. The third loop comprised DCMD, which was composed of three modules with a total area of 3.39 m². The fourth loop comprised a thermal sink with a cooling water capacity of 10³ L/h. The distillate rate per module was 3.31 and 4.59 L/h for with and without a heat-recovery device, respectively. Lee et al. [17] theoretically studied the short- and long-term performances of a solar-driven multi-stage DCMD system. The mid-latitude meteorological data from Busan, South Korea were used to emulate the climate variation over a 1 y period. The enhancement of both water production and thermal efficiency was studied by dynamically changing the number of module stages. The water production per day improved from 0.37 to 0.4 m³/d, and thermal efficiency increased from 31% to 45%, when shifting from static to dynamic operation.

Schwantes et al. [18] experimentally focused on full-scale modal systems by using a parallel multi MD-module configuration. Three process schemes were proposed, where one used low-grade energy, and the other two operated using solar thermal collectors. The impacts of operating conditions, such as feed-flow rates, salt composition, operation duration, and process temperatures, were considered. Chung et al. [19] theoretically studied multistage vacuum membrane distillation (MSVMD) for zero liquid discharge applications. Energy, second law efficiencies, and specific membrane area were the key metrics to assess the system performance. The outcomes indicated that the MSVMD system could be as efficient as conventional MSF plants for a wide range of feed concentrations. Khayet [20] conducted a comprehensive and critical review of energy consumption and water cost for MD-based solar desalination. The estimated specific energy consumptions by various MD systems varied from 1 to approximately 9,000 kWh/m³, thereby raising a real concern on the actual energy management in the aforementioned desalination systems.

Based on results reported on solar-energy-driven MD technologies [11,14–17,18] the thermal-energy consumption ranged from 200 to 2,200 kWh/m³. However, no indication was given on the electric energy consumed. The reasons of the aforementioned dispersion in the energy-consumption rates can be obviously associated with not only the design specifications and high/poor performance of the systems considered, but also with the types of energy considered and the methods adopted to evaluate such energy rates. Based on the above-reviewed studies and a more comprehensive review of solar-driven MD systems conducted by the authors, one can conclude that the number of studies on solar MD units is increasing, thereby showing the potential of MD as a desalination process integrated with solar energy. Moreover, the dispersion of the specific energy consumption rates of the desalinated water using MD technology is reported. Furthermore, the recovery ratio obtained by a single MD is considerably low. Therefore, efforts are directed toward improving the recovery ratio by using cascaded MD systems such as vacuum multi-effect membrane distillation (V-MEMD).

Recently, some contributions regarding solar-energy-powered V-MEMD systems have been reported. Ong et al. [21] experimentally investigated the performance of the MEMD desalination by reusing the waste heat recovered from a high-concentration PV thermal system. Their goal was to attain the co-generation of both electricity and freshwater, where the feed temperature was maintained between 75°C and 80°C during 24 h via thermal-energy storage. The results indicated that productivity could reach 3 m³/d. Reusing the recovered waste heat helped in maximizing the gain output ratio (GOR) to approximately 4.3 and reducing the specific thermal-energy consumption (STEC) to 128.1 kWh/m³. Zhao et al. [22] reviewed the effect of the solar and diesel heater coupled with a V-MEMD system. The results showed that heating and cooling temperatures were the main factors that affected both permeate flux and energy efficiency. In addition, they found that the potential of the V-MEMD unit was significant for enhancing GOR. Zaragoza et al. [23] studied the performances of solar thermally driven commercial prototypes of different MD technologies

experimentally using various configurations, that is, air gap, permeate gap, and vacuum, with flat plate and spiral wound membranes. They observed that the permeate flux could approach 14 kg/m^2 h with a high recovery ratio of a maximum of 58% and 59% for seawater and brackish water, respectively. Mohamed et al. [24] experimentally studied the performance indicators of the V-MEMD system on the basis of outdoor operating conditions and the overall design by considering local economic conditions. The productivity of the V-MEMD unit mainly increased with an increase in the heating water temperature, reaching a maximum of 50 L/h at 80°C. Notably, STEC, GOR, and performance ratio (PR) were in the range of 300–700 kWh/m^3, 1.0–2.2, and 0.4–0.9 kg/MJ, respectively. Boutikos et al. [25] developed a mathematical model to predict the guidelines of the optimal design and operation of a V-MEMD system. The optimum values of productivity, recovery ratio, GOR, and STEC were estimated to be 32 L/h, 40%, 2.63, and 252 kWh/m^3, respectively. Lastly, Andrés-Mañas et al. [26,27] remarkably modified a V-MEMD module by using the seawater feed flow as a cooling medium in the condenser, rather than using a separate circuit. Their idea was to enhance the productivity and reduce the heat applied on the V-MEMD unit; therefore, the maximum permeate flux reached 8.5 L/m^{2}h, and GOR reached 3.2 correspondings to the hot water temperature of 75°C, with the feed capacity of 150 L/h.

In this paper, we summarize the experimental results on the performance of a solar-driven desalination system based on V-MEMD, in Riyadh city. The results are expressed in terms of the variations in the following: recovery ratio, GOR, PR, specific electric energy, and specific thermal energy consumed. In addition, we focus on the thermal and electric energies consumed by various constituents of the solar desalination system.

2. Configuration of the integrated solar-driven desalination system

The system is constructed such that it can operate as a stand-alone unit in arid or semi-arid isolate regions. It is compact for ensuring easy installation and deployment. For portability purposes, a modified 6.0 m × 2.4 m × 2.6 m container was used to house all the equipment, with the exception of the PV array. Fig. 1a depicts the system set up inside the holder. Figs. 1b and c depict the PV array and solar thermal collectors, respectively. The feed tank can hold up to 10,000 L of saline water. The stored saline water (seawater or brackish water) is used as feed and also for cooling. Prior to filling the feed tank, the saline water was prefiltered via hollow fiber ultrafiltration. Fig. 1a depicts a heat pump mounted inside the container. The heat pump conveys heat from a cold space/stream to a warmer stream. It moves heat instead of generating heat, thereby consuming considerably less amount of electricity than that consumed by the conventional heater and/or cooler. In this study, the heat pump has the following two functions: preheating the feed water and cooling down the cooling water during unit operation. The functions are performed by transferring heat from the cooling stream to the feed stream. The used refrigeration system is a direct-expansion water-cooling system (single cycle).

It cools the fluid of the condenser circuit during high-load conditions, that is, summer months during which the inlet heating temperature exceeds 55°C. However, during winter, when the inlet heating temperature is as low as 55°C, the refrigeration system is disabled, and tap water at ambient temperature is used in the condenser circuit. The schematic of the solar-driven desalination system is shown in Fig. 2. The existing setup comprises the following three main elements: a solar-PV system, solar–thermal system, and MEMSYS V-MEMD unit (Germany) [28]. Each sub-system is described in the following sections. More details on each constituent and on the operation of the overall system are given in Chafidz et al. [28].

2.1. Solar-PV system

The solar-PV unit supplies electricity required to run all electrical devices such as pumps, motorized valves, and sensors. Its major elements are a PV panel, charge controller, battery pack, DC/AC inverter, DC/DC converter, and DC shunt. The PV array and its accessories are illustrated in Fig. 1b. The PV array is installed in a fixed orientation (without solar-trajectory tracking). The solar-PV system uses the charge controller with an MPPT to leverage electricity by using the PV array to power the solar-driven desalination system and charge the battery. The battery stores the surplus electrical energy for ensuring extended system operation after sunset. The first six items in Table 1 are the equipment used in the solar-PV system. An installed DC/AC converter inverts the 48 V DC to 230 V AC, which is required by "high-load" equipment such as pumps, whereas a DC/DC converter converts 48 V DC from the battery to 24 V DC, which is used by the sensors and programmable logic controllers (PLCs). In addition, three DC shunts were also installed to measure the magnitude of the current flows across the individual shunts. Further details can be found in Chafidz et al. [28].

2.2. Solar–thermal system

The solar–thermal system has the following five major units: a solar thermal collector, thermal storage tank, heat exchanger, thermal pump, and V-MEMD unit pump, as depicted in Figs. 1a and c. A list of equipment used in the solar–thermal system is presented in Table 1 (items 7–14). The thermal collectors collect heat (thermal energy) by absorbing radiation from the sun. The thermal energy collected is used to heat the freshwater (heat-transfer fluid) in the thermal storage tank. The water is circulated through the collector via the thermal circuit pump until it reaches the high-temperature range of 60°C–90°C. In the auto mode, the water flow rate is regulated via a PLC to optimize the thermal energy harnessed by adjusting the speed of the thermal pump. As the temperature approaches the target temperature, the V-MEMD unit becomes operational to provide thermal energy to the evaporator (steam raiser). The operation is attained by pumping the hot water from the tank through a plate heat exchanger. The thermal storage tank works as a buffer to attenuate weather oscillations and stock the excess heat. The tank is well-insulated using polyurethane foam. The maximum allowable tank temperature

(a)

(b)   (c)
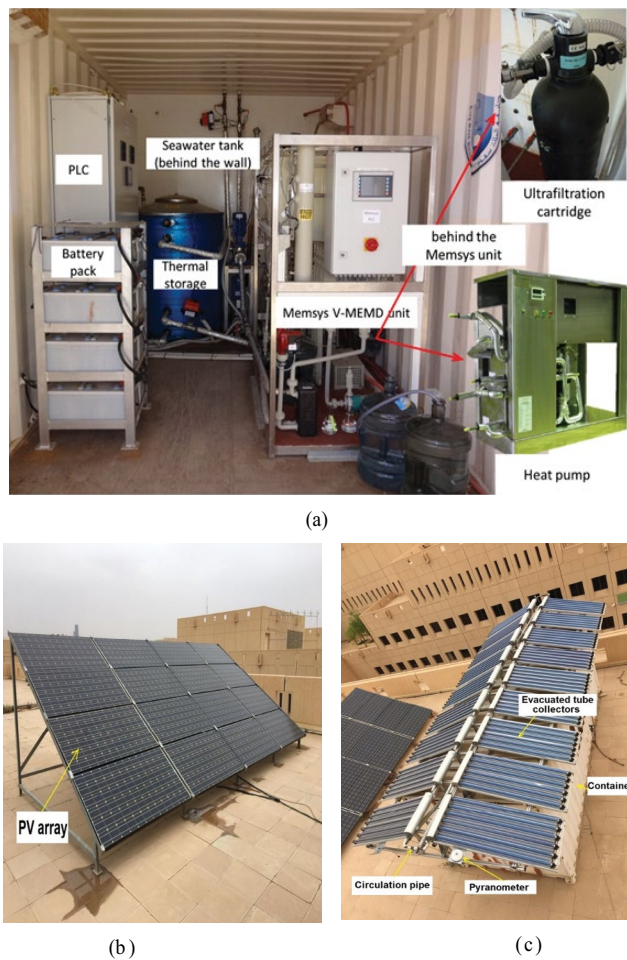
Fig. 1. (a–c) Photographs of system facilities.

is 95°C. Evacuated tube collectors, which are used as solar thermal collectors (CPC 1506), are mounted atop the container. Fig. 1c depicts the solar thermal collectors.

2.3. Vacuum multi-effect membrane distillation

The V-MEMD system is the main component of the solar-driven desalination unit. It integrates the benefits of both the MED process and membrane-separation process to formulate a compact modular structure that runs in a vacuum and uses thermal-energy recycling. It works on the principle of the VMD process, as depicted in Fig. 1a. The VMD process keeps the pressure on the permeate side under the saturation vapor pressure by applying negative pressure (vacuum). The vacuum promotes the driving force (vapor-pressure difference) through the membrane. Because the V-MEMD system operates at moderate temperatures and negative pressure, the entire pipeline can be built using plastic. The hydrophobic membrane is made of polytetrafluoroethylene with a pore size of approximately 0.2 μm. The size of the single flat-sheet is 335 mm × 475 mm. The membranes are welded in PP frames. The V-MEMD system comprises frames and stages, and several stages are jointly sealed to produce a single module. Fig. 2 depicts the principle of the V-MEMD process. The V-MEMD system contains the following three major elements: a steam raiser (evaporator), multiple stages (evaporation–condensation), and a condenser. The steam raiser comprises numerous layers of membranes and is mounted before the foremost stage. It supplies the thermal energy required for the V-MEMD process. The steam raiser has a plate heat exchanger to exchange heat with the hot water coming from the thermal storage tank. Consequently, the feed freshwater evaporates in the steam raiser at the pressure lower than 200 mbar. The steam (hot

Table 1
Equipment in the PV system of the integrated desalination system

No.	Item	Quantity	Specification
1	PV module	16	Maximum power (P_{max} = 3.36 kw)
2	Solar-battery charger with maximum power point tracker (MPPT)	2	Maximum 60 amps continuous battery current, maximum solar input 12, 24, 36, and 48 VDC
3	Battery pack	8	12 V 170 Ah lead acid battery
4	AC/DC inverter	1	Output: rated power (typ) 3,000 W, sine wave, 50–60 Hz, 200–240 VAC, and input: 48 V, 75 A
5	DC/DC converter	1	Rated power (typical) 504 W, 24 VDC, 0–12 A, and input: 19–72 VDC
6	DC shunts	3	Sensing element: Manganin
7	Solar thermal collectors	18	Evacuated tube collector CPC 1506 (six tubes and area A = 1 m^2 for each)
8	Thermal storage tank	1	600 L capacity, with inner tank SUS 316 L (0.5 mm) and outer tank made of Zn–Al (0.4 mm) with 50 mm polyurethane foam insulation
9	Circulation pump	2	Rated power 0.37 kW/0.5 HP
10	Heat exchanger	1	Plate heat exchanger
11	Temperature sensor	3	Pt 100
12	Flow meter	2	Measuring range 0.01–6 m^3/h
13	Motorized valve	2	Power 14 W, rotation angle (0°C–90°C)
14	Floating switch	1	Three floating sensors located at 5, 60, and 115 cm
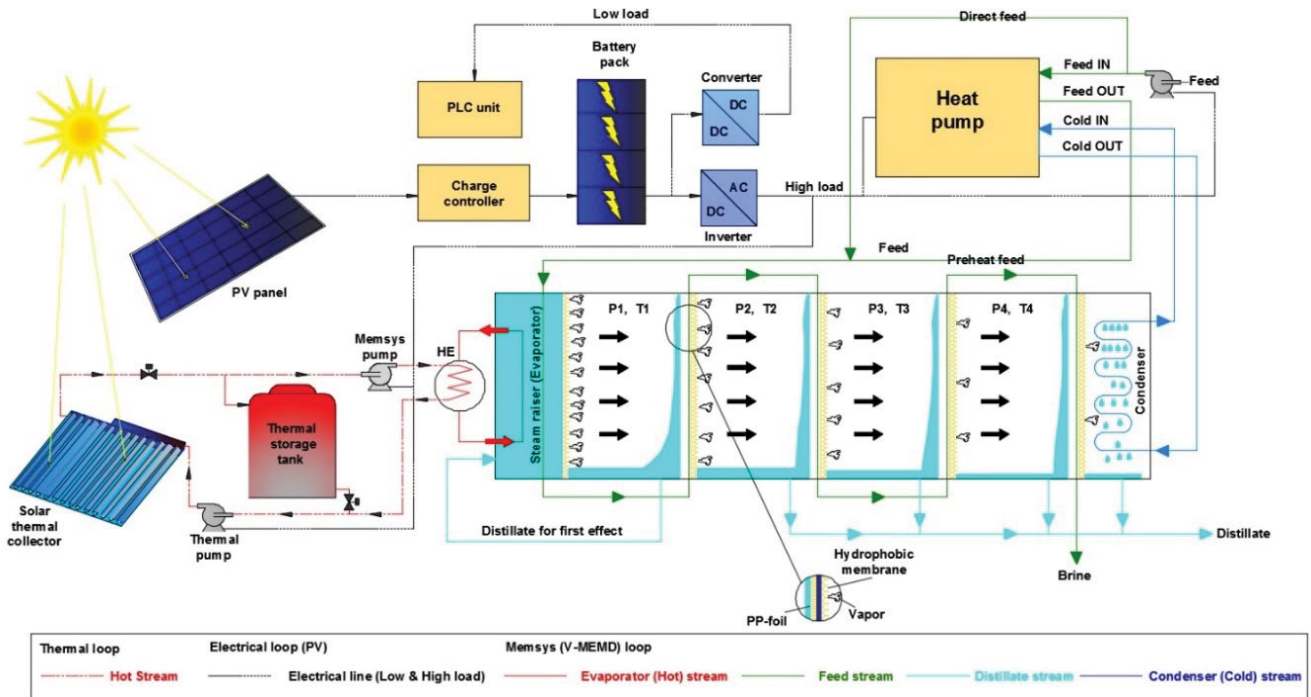
Fig. 2. Schematic of system facilities.

vapor) generated moves to the first stage of the cascaded (evaporation–condensation) chambers. As water evaporates, additional water is fed to refill the steam riser. Because the system operates in vacuum conditions, the water produced from the distillate tank can be sucked into the internal heating loop with a tube and then used as a refill. The V-MEMD module used in this study comprises four effects (stages). The heat of condensation for the evaporation process at the subsequent stage is recovered in each effect; this process is repeated at subsequent stages at a reduced temperature. The condenser is fabricated using several foil layers and performs the condensation of the vapors produced in the terminal stage. Further details on V-MEMD can be found in Chafidz et al. [28]. The system includes an ultrafiltration cartridge made of hollow fiber (hydrophilic modified PAN) to prefilter the tested water while filling the feed tank. For all the conducted experiments, the quality of the distillate was examined using portable meter from HANNA, which indicated the conductivity measurements of less than 10 μS, corresponding to the salinity of less than 5 ppm according to our calibration.

2.4. Control system

The automation, control, and monitoring of the system are governed using two PLCs, a Schneider PLC, and a BnR PLC. The Schneider PLC controlled the solar-PV and solar–thermal systems, whereas the BnR PLC controlled the V-MEMD module. In addition, the control system included two human–machine interfaces (HMIs) and two variable speed drives (VSDs). The HMIs permit the operator to run the process in different modes such as the auto and manual modes. The VSDs usually regulate the frequency (speed) of

the pump motors as required. A prespecified built-in control algorithm was used to govern the VSD for controlling the speed of both the thermal pump and V-MEMD unit pump. It should be noted that after each experiment, the system is washed using the cleaning procedure given in the supplement material. The purpose of the cleaning procedure is to avoid fouling and hence maintaining the life cycle of the system.

3. Experiment results and discussion

3.1. Weather conditions

The experiments on the solar distillation system were performed during several days of 6 different months, namely, June, November, December, February, March, and April (years 2017–2018), in Riyadh. As an example, Fig. 3a shows the results of global solar irradiations obtained on the typical days of the aforementioned months, during which the system performed for approximately 6–8 h from 08:00 AM to 04:00 PM. The maximum global irradiations for each of June, November, December, February, March, and April are depicted in Fig. 3a. A similar trend is observed for some of the months, with noticeable fluctuations during early hours and smoother variations later. The corresponding maximum air temperature of several working days were 39.6°C, 29.2°C, 27.6°C, 31.2°C, 35.4°C, and 36.3°C, respectively, as shown in Fig. 3b. Intuitively, the temperature of the thermal storage tank is directly related to the weather conditions during the experiment, and therefore, the triggering temperature, that is, the thermal storage tank temperature of the experiment can be achieved at as early as 12:00 PM in June, February, March, and April, while it delays by an

hour, that is, between 01:00 PM and 01:30 PM, in November and December, as will be described in the next section.

3.2. Performance of the solar–thermal collectors

Fig. 4 depicts the variations, during a typical day (10 April 2018), in the main variables, such as the thermal storage tank temperature, evaporator (steam raiser) temperature, effects temperatures, and cumulative distillate water, of the solar–desalination system. The thermal storage tank temperature is approximately 40°C in the early morning and reaches approximately 81.9°C at 12:30 PM. The desalination unit begins operation by using the heat accumulated in the storage tank when its temperature reaches the desired (prescribed) temperature (greater than 65°C). The temperature profiles of the effects have two patterns.

The first pattern is observed when the temperature exhibits sharp fluctuations during a short time of approximately 1 h. Subsequently, the second pattern is observed when the temperatures tend to become more stabilized until approximately 04:30 PM. The initial fluctuation in the temperature measurement is attributed to the startup operation of the process, creating disturbances until the system reaches steady operation. Notably, the process is triggered when the storage-tank temperature reaches the desired value, as mentioned earlier. We must mention that the difference between the condenser temperature and the inlet cooling temperature seems to be high. However, the freshwater production begins at approximately 01:30 PM with a delay of more than 5 h from the starting of the experiments, thereby showing the importance of system inertia. The amount of distillate water linearly increases to reach 80 L at the end of the day.
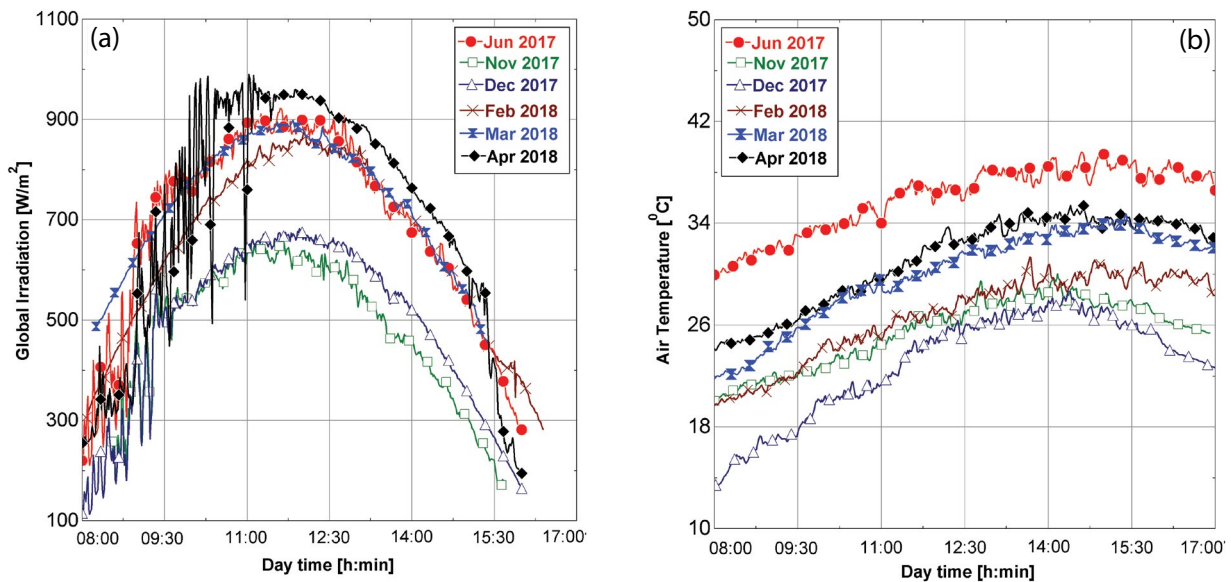
Fig. 3. Measured hourly (a) global irradiations and (b) air temperatures during the tests; (8 AM–4 PM) at KSU.
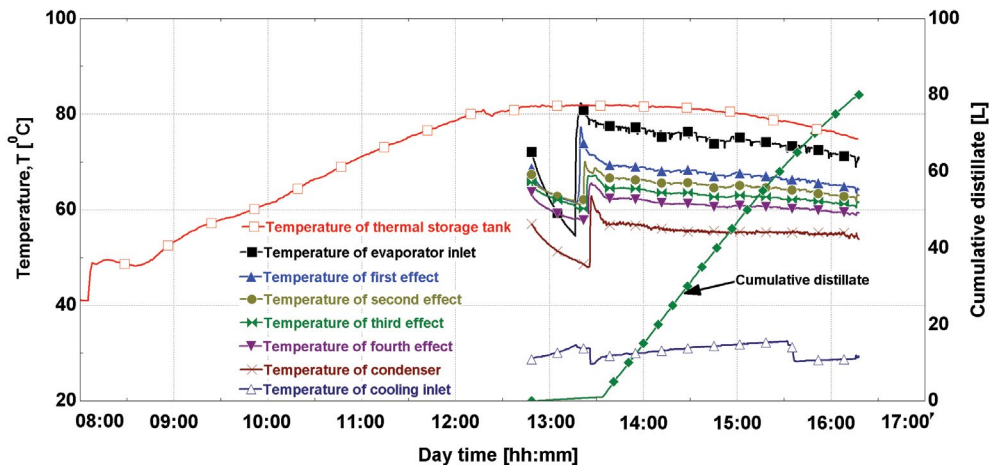
Fig. 4. Experimental results of the solar–desalination system on April 10, 2018.

Several tests similar to that depicted in Fig. 4 were conducted over different months. The summary of the testing days in 6 different months, in terms of weather data and thermal-energy information, is described in Table 2. The graphical presentation of these data is given in the supplementary material and shown in Fig. S1. The maximum temperature of the thermal-storage tank reached approximately 74.1°C–81.9°C in tests for June, February, March, and April and 66°C–67.1°C in tests for November and December. The corresponding inlet heating temperatures for the aforementioned 2 tested month groups are 65°C–75°C and 55°C, respectively. Therefore, for high $T_{h,in}$, the refrigeration system is turned on and for low turned off, as mentioned earlier. The temperature profiles of these tests are not shown here to limit the number of Figs, as they are almost similar to that in Fig. 4. However, a summary of these results is discussed in the following. The maximum temperature of the thermal-storage tank was achieved at as early as 12:00 PM (i.e., 4 h from the start of the experiment) in June, February, March, and April, whereas it was achieved at approximately 01:00 PM to 01:30 PM (i.e., 5–5.5 h from the start of the experiment) in November and December. Therefore, it can be concluded that the productivity period of the V-MEMD unit decreased significantly in November and December compared with other months. In all the cases, the operation period lasted until 04:00 PM. Subsequently, the experiments were halted, as the global irradiation decreased, and thermal-storage tank temperature sharply decreased. The temperature loss between the thermal storage tank and inlet evaporator was attributed to the insufficient insulation around the connecting pipe. In addition, the temperature difference between the inlet and outlet heating (evaporator) of the V-MEMD unit was lower than 5°C in the November and December days and 10°C in the June, February, March, and April days. The heat consumed by the V-MEMD unit varied for the given months depending on the input conditions. Therefore, its values were significantly high in the June, February, March, and April days, and minimal in the November and December days. During the freshwater-production period, a high-temperature drop means large permeation flux under vacuum, thereby requiring more vaporization heat. Furthermore, the system could not continue efficient operation after 04:00 PM, as the temperature of the thermal-storage tank considerably decreased.

3.3. Performance of the V-MEMD unit

To understand water production and performance of the V-MEMD unit, different indicators were evaluated. Brackish water with the salt concentration of approximately 1,260 ppm (1.260 g/kg) was used. The cold-stream water temperature was maintained to be constant using the refrigeration system, as depicted in Fig. 4, especially at high heating (evaporator) temperatures of 70°C–75°C. The profile of the cold-stream water exhibited slight variations due to temporary fluctuations in the source. Notably, during high-load conditions, the temperature of the inlet cold water was maintained at 25°C–30°C and at 18°C–21°C during low-load conditions. Therefore, we consider that the V-MEMD performance presented in this study is valid within the given range of the cooling-water temperature. Temperatures, pressures, flows (i.e., feed, distillate, and brine) were monitored and recorded using the BnR PLC controls. The system offers two control modes of the feed temperature. The first one is called the direct mode, wherein the feed temperature is the same as that of the feed tank, while the second mode is called the preheat mode, where feed stream exchanges heat with a heat pump, as depicted in Fig. 2.

For analyzing multiple effects, the ratio of water production to the area of a hydrophobic membrane surface (kg/m² h) is a sensible metric for comparison. The mass flux *J* is calculated as follows:

$$J = \frac{v_d^0 \times \rho_d}{A} \tag{1}$$

where v_d^0 and ρ_d denote the distillate volume flow rate and distillate density, respectively, and *A* is the membrane area. The recovery ratio (*R*) is used to evaluate the amount of the distillate water produced from the supplied feed water, and it is often defined as follows [29]:

$$\%R = \frac{v_d^0}{v_f^0} \times 100 \tag{2}$$

Notably, GOR is useful to assess the performance of the V-MDMD unit and is plotted, for example, as a function of the inlet heating (evaporator) temperature. It is calculated as follows [30]:

Table 2
Summary of weather data and thermal-energy information for the solar collection, storage systems, and heat consumed by the V-MEMD unit, for several testing days

Test	Months	Global irradiation		Solar thermal power		Triggering temperature	Inlet heating (evaporator) temperature	Heat consumed by the V-MEMD unit
		I_{max} (W/m²)	I_{avg} (W/m²)	Q_{max} (W)	Q_{avg} (W)	T_{tank} (°C)	$T_{h,in}$ (°C)	Q_h^0 (W)
A	June	922.5	687.2	6,083	4,561	Approximately 78.8	75	4,398–5,501
B	November	658.9	488.6	3,335	2,280	Approximately 67.1	55	2,525–2,938
C	December	682.2	486.3	4,639	3,008	Approximately 66.0	55	2,525–2,938
D	February	877.6	649.1	6,726	5,028	Approximately 74.1	65	3,063–3,842
E	March	898.7	736.8	6,526	5,830	Approximately 78.7	70	3,854–4,023
F	April	990	700.3	7,342	5,934	Approximately 81.9	75	4,398–5,501

$$\text{GOR} = \frac{v_d^0 \rho_d (T_d, P_a) h_{fg}(T_d)}{Q_h^0} \qquad (3)$$

In the next section, the experimental results of the solar-driven desalination system over the possible range of the heating (evaporator) temperature $T_{h,in}$ are analyzed. The heating (steam raiser) temperature ranges from 55°C to 75°C; these temperature values are the maximum attainable values that can be achieved during June, November, December, February, March, and April. The other design parameters are kept constant during the experiments. For example, the evaporator flow rate of the heating loop, v_h^0, is fixed at 840 L/h; the condenser flow rate of the cooling loop, v_c^0, is fixed at 405.5 L/h; the inlet cooling (condenser) temperature $T_{c,in}$ is set between 25°C and 30°C; the feed-flow rate v_f^0 is set to 87 L/h. During the experiments, the salinity in the feed tank was kept constant because the concentrated brine was rejected, and the cold-side absolute pressure P_v was operated in the range of 75.4–163.7 mbar. The results are illustrated in Figs. 5–9, which show the response of various performance indicators. Fig. 5 demonstrates how the feed flow rate affects the first effect temperature and consequently the production rate negatively. Notably, Mohamed et al. [24] reported similar behavior, as they observed that the production rate decreased upon increasing the feed-flow rate. This observation can be explained by the fact that increasing the flow rate decreases the residence time and increases the thermal capacitance of the feed stream. Therefore, the feed stream became less heated, resulting in lower evaporation.

As depicted in Fig. 6, mass flux J, recovery ratio R, and GOR increase almost linearly with increased inlet heating (evaporator) temperatures. Generally, the average reduction percent in J, R, and GOR due to feed-flow increment is approximately 21.5%, 51.1%, and 23.2%, respectively. Expectedly, the recovery ratio R is higher at lower feed-flow rates v_f^0. In addition, for low evaporator temperature $T_{h,in}$,

the effect of the feed-flow rate is not as significant as for high $T_{h,in}$. Such behaviors of R, $T_{h,in}$, and v_f^0 have also been observed in [24]. However, as shown in Fig. 6a, the permeate flux J increases with $T_{h,in}$, with a larger slope than that for the case of the recovery ratio, R. The permeate flux can reach approximately 12 kg/m² h for the $T_{h,in}$ of 75°C and v_f^0 of 87 L/h. Increasing the feed-flow rate reduces the permeate flux J for the same reasons mentioned earlier in Fig. 5. Fig. 6b depicts the impact of $T_{h,in}$ on GOR for two feed-flow rates. The performance indicator, namely, GOR is strongly linked to the permeate flux J. GOR increases from 1 to 4.25
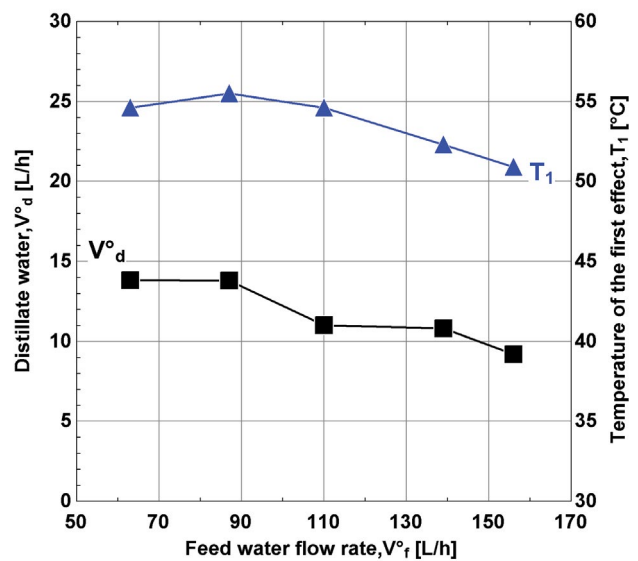
Fig. 5. Effect of the feed-flow rate, v_f^0 on distillate water and temperature of the first effect (v_h^0 = 840 L/h; $T_{h,in}$ = 60°C; v_c^0 = 405.5 L/h; $T_{c,in}$ = 25°C–30°C; $T_{f,in}$ = 27°C–40°C; S_f = 1,260 ppm; P_v = 98.24–112.2 mbar).
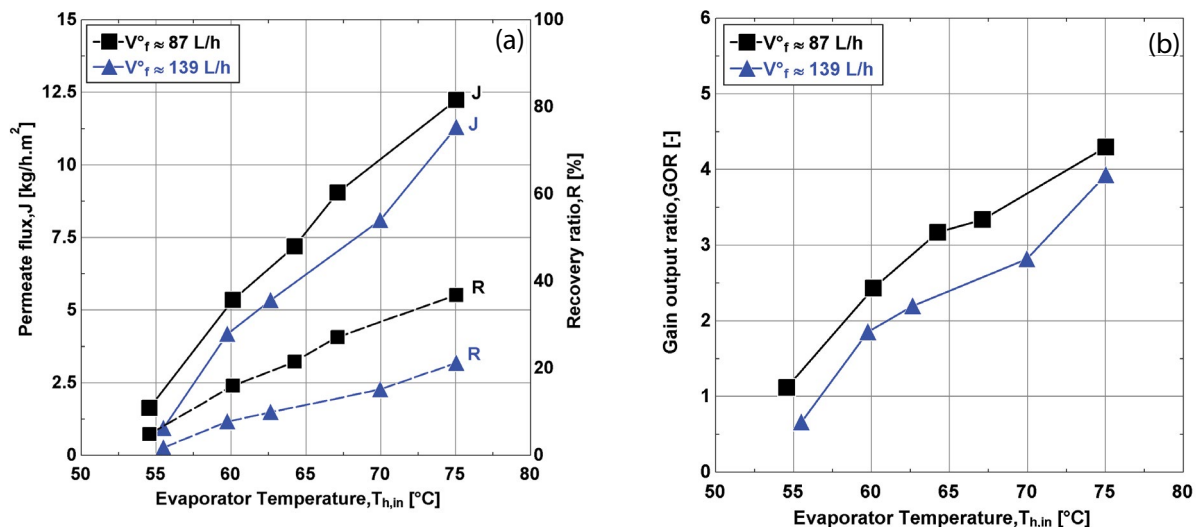
Fig. 6. Effect of the evaporator temperature $T_{h,in}$ on: (a) permeate flux and recovery ratio and (b) GOR for different feed-flow rates, (v_h^0 = 840 L/h; v_c^0 = 405.5 L/h; $T_{c,in}$ = 25°C–30°C; P_v = 75.4–163.7 mbar; S_f = 1,260 ppm; preheat mode).
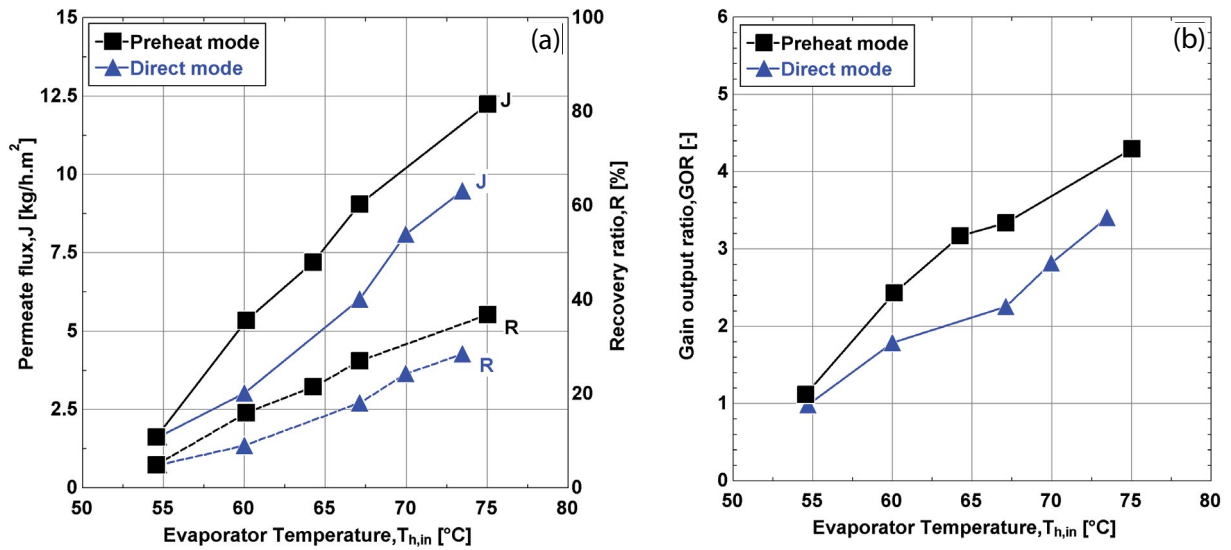
Fig. 7. Effect of the evaporator temperature $T_{h,\text{in}}$ on: (a) permeate flux and recovery ratio and (b) GOR for different feed modes, that is, different feed temperatures (v_h^0 = 840 L/h; v_c^0 = 405.5 L/h; $T_{c,\text{in}}$ = 25°C–30°C; P_v = 75.4–163.7 mbar; S_f = 1,260 ppm; v_f^0 = 87 L/h).
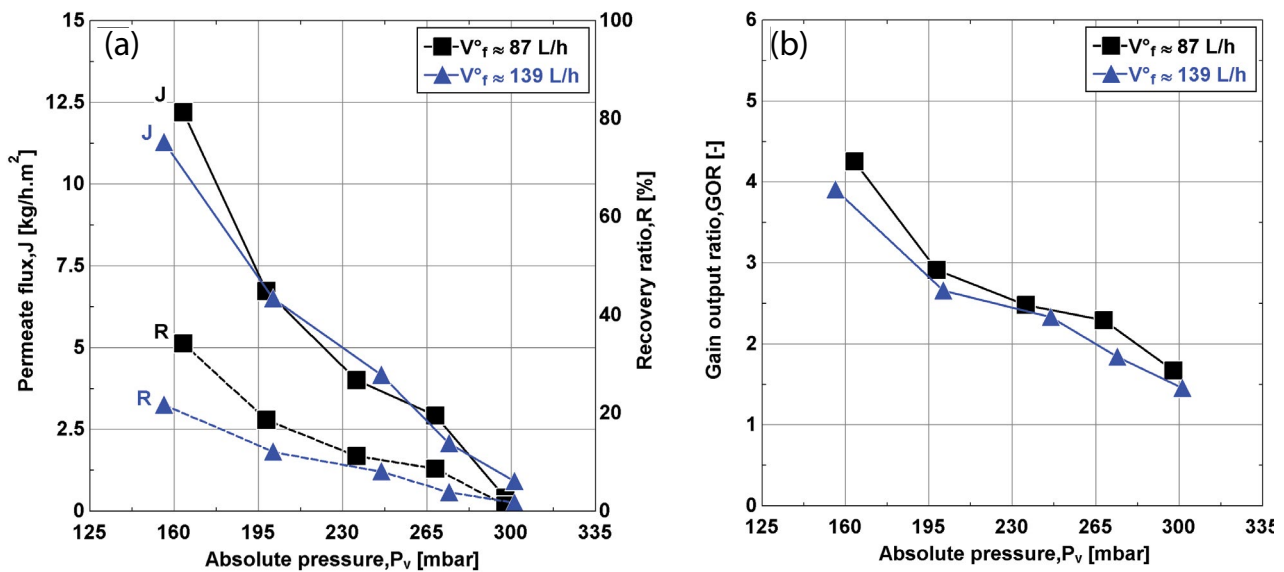
Fig. 8. Effect of the cold-side absolute pressure P_v on (a) permeate flux and recovery ratio and (b) GOR for different feed flows (v_h^0 = 840 L/h; $T_{h,\text{in}}$ = 74.9°C; v_c^0 = 405.5 L/h; $T_{c,\text{in}}$ = 25°C–30°C; preheat mode; S_f = 1,260 ppm).

as the evaporator temperature rises from 55°C to 75°C. Ong et al. [21] obtained GOR values ranging from 3.8 to 4.3.

Fig. 7 depicts the effect of preheating the feed-flow rate on the system-performance indicators. The benefits of preheating the feed water are considerably important for high evaporator temperatures $T_{h,\text{in}}$. Particularly, for the $T_{h,\text{in}}$ of 55°C, no significant improvement was registered. When the inlet heating (evaporator) temperature reached approximately 75°C, the enhancement percentages in mass flux J, recovery ratio R, and GOR due to the feed-stream preheating could reach 22.5%, 22.5%, and 20.7%, respectively.

Notably, during some experiments when the refrigerating system was not running, the V-MEMD unit could not

produce distillate water because of the increase in the inlet cooling (condenser) temperature, especially at high heating (evaporator) temperatures ranging from 70°C to 75°C, indicating that the fresh-water production was controlled by various parameters such as the hot source temperature and cooling temperature. The refrigeration system is critical to enhancing the distillate-water production, as described in Table 3. One can see that upon enabling the refrigeration system, all the performance indicators notably increase for both the values of $T_{h,\text{in}}$ close to 70°C and 75°C. In addition, the water-production duration expands. Specifically, Table 3 indicates that when the cooling system is not active, the drops in the production rate, mass flux, recovery ratio, and
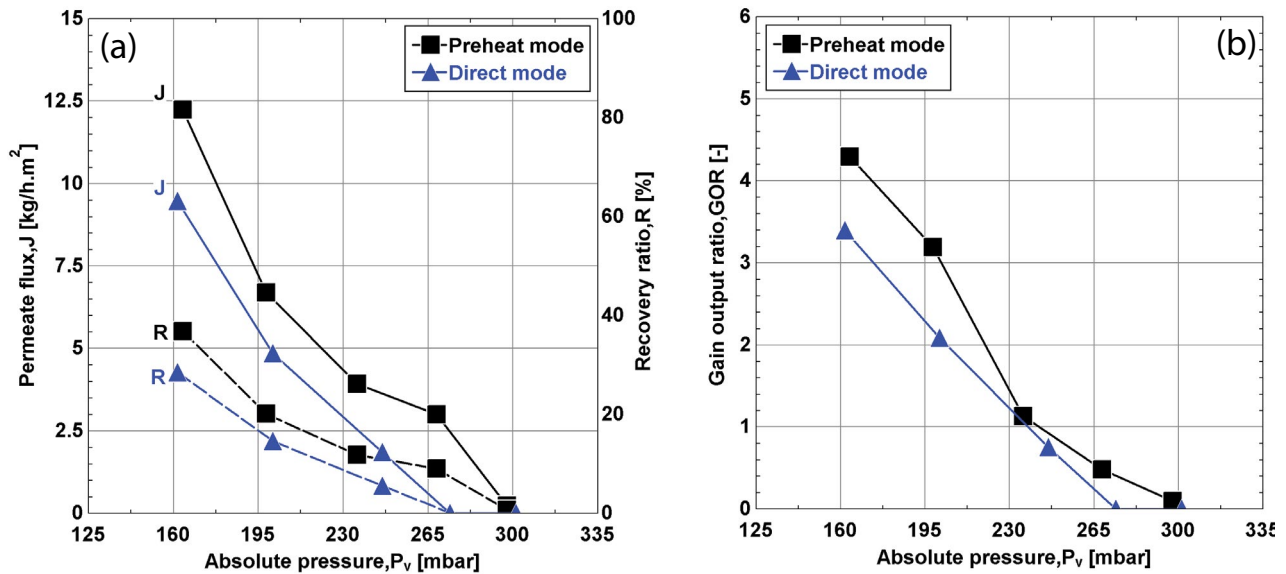
Fig. 9. Effect of the cold-side absolute pressure P_v on (a) permeate flux and recovery ratio and (b) GOR for different feed modes, that is, different feed temperatures (v_h^0 = 840 L/h; $T_{h,\text{in}}$ = 74.7°C; v_c^0 = 405.5 L/h; $T_{c,\text{in}}$ = 25°C–30°C; v_f^0 = 87 L/h; S_f = 1,260 ppm).

Table 3
Effect of the refrigeration system on some of the experiments

Test case	Inlet heating (evaporator) temperature, $T_{h,\text{in}}$ (°C)	Refrigeration system	Time duration of water production (h^0:min)	Productivity, v_d^0 (L/h)	Mass flux, J (kg/m² h)	Recovery ratio, R (%)	Gain output ratio, GOR (–)
A	69.12	Yes	4^0:02	Approximately 26.2	9.92	29.8	3.40
B	69.95	No	1^0:01	Approximately 21.7	8.08	24.3	2.80
C	75.7	Yes	3^0:31	Approximately 31.8	12.2	36.8	4.25
D	75.03	No	1^0:30	Approximately 28.8	11.05	33.3	3.85

GOR are 9.4%–17.1%, 9.4%–18.5%, 9.5%–18.4%, and 9.4%–17.6%, respectively.

As depicted in Fig. 8, the cold-side absolute pressure is critical in enhancing the mass productivity and the overall performance of the V-MEMD unit. Notably, low P_v significantly increases the mass transfer of water vapors, thereby resulting in a significant driving force. Generally, all the performance parameters, namely, J, R, and GOR decrease with increasing P_v. However, they do not decrease linearly; that is, they may have different rates of change for every 35 m bar change in P_v. For example, J can decrease by as much as 5.56 kg/m² h or as low as 1.07 kg/m² h for a 35 m bar step-change in P_v. Similarly, the reductions in R, and GOR can be in the ranges of 2.21%–15.6%, and 0.18%–1.39%, respectively. The effect of the feed-flow rate on J is minor, except at considerably low P_v; this effect becomes more noticeable for the recovery ratio at low P_v. GOR shows minor differences that do not exceed 0.46, as depicted in Fig. 8b; the minor differences can be attributed to the reduction in thermal-energy expansion on the units.

Fig. 9 depicts the influence of flow modes on the process performance, over a specific range of P_v. Compared to the effect of feed-flow rate as depicted in Fig. 8, the preheat mode affects the performance indicators more notably. As the cold-side absolute pressure increases, the thermal energy in the steam raiser (evaporator) compartment cannot effectively expand to the last effect where cooling (condenser) is located. However, at P_v equal to 160 mbar, GOR when preheat is enabled can be enhanced by 26.6% over that for the direct mode.

3.4. Overall system performance

We focus on both electrical and thermal energy consumed by the main components of the solar distillation system. The total amount of electricity consumed in the operation of the experiments performed in November, December, and February were approximately 5.32, 5.68, and 6.18 kWh, respectively. However, in June, March, and April, the registered electrical-energy consumption was 11.88, 9.52, and 11.88 kWh, respectively. Notably, electrical consumption was recorded using the system instrumentation. Such an increased energy consumption during the summer months compared with that during the winter months is attributed to the refrigeration system required to maintain the temperature of the condenser at a fixed and low value. Fig. 10
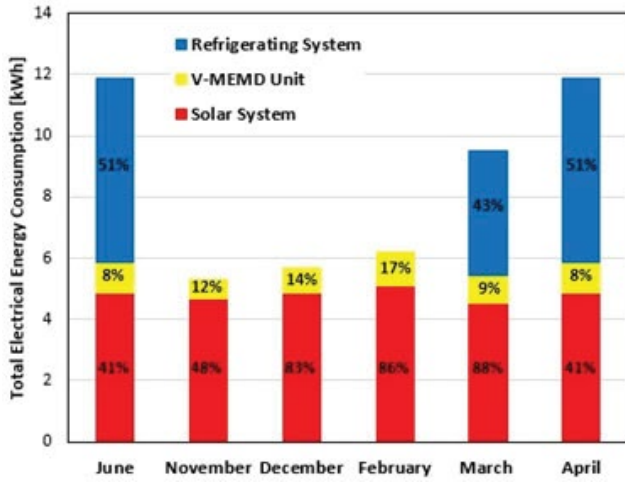
Fig. 10. Electrical-energy consumption for each system element, that is, the solar system, V-MEMD unit, and refrigerating system.

shows the electrical-energy-consumption distribution for each sub-system of the solar desalination system. For more analysis, we divided the solar desalination system into the following three main sub-systems. The first sub-system is denoted as thermal (solar system). The second sub-system is called the V-MEMD unit, which contains several pumps (i.e., heating (evaporator), feed-I, feed-II, brine, distillate-I, distillate-II, vacuum, cooling (condenser) pump), and auxiliaries. The third sub-system corresponds to the refrigeration unit, which is used to cool the V-MEMD unit, and it is often used during summer days (i.e., during June, March, and April). Fig. 10 shows that the desalination unit (V-MEMD) consumes the lowest percentage of energy, that is, between 8% and 17% of the total electric energy of the whole system. The cooling process (refrigeration unit), which operates only in summers, requires a high amount of electric energy.

The specific electrical-energy consumption (SEEC) was used to evaluate the amount of electric energy required to produce one cubic meter of distillate water, and it is defined as follows:

$$\mathrm{SEEC}_{V-\mathrm{MEMD}} = \frac{\sum E^0_{V-\mathrm{MEMD}}}{v^0_d} \tag{4}$$

Also,

$$\mathrm{SEEC}_T = \frac{E^0_S + E^0_R + E^0_{V-\mathrm{MEMD}}}{v^0_d} \tag{5}$$

where E^0 denotes the amount of electric energy rate consumed. In addition, E^0_S, E^0_R, and $E^0_{V-\mathrm{MEMD}}$ denote the electric energies consumed by the solar system (i.e., thermal pump, MEMSYS pump, and motor valves), heat-pump (refrigerating) system, and V-MEMD components (i.e., heating pump, feed pump, cooling pump, brine pump, distillate pump, vacuum pump, and auxiliaries). However, the evaluation of STEC requires the evaluation of the thermal energy supplied to the V-MEMD unit, Q^0_h, which can be calculated using the following energy balance equation [15]:

$$Q^0_h = v^0_h \begin{bmatrix} \rho_{h,\mathrm{in}}\left(T_{h,\mathrm{in}}, P_{h,\mathrm{in}}\right) \cdot h_{h,\mathrm{in}}\left(T_{h,\mathrm{in}}, P_{h,\mathrm{in}}\right) - \\ \rho_{h,\mathrm{out}}\left(T_{h,\mathrm{out}}, P_{h,\mathrm{out}}\right) \cdot h_{h,\mathrm{out}}\left(T_{h,\mathrm{out}}, P_{h,\mathrm{out}}\right) \end{bmatrix} \tag{6}$$

STEC gives the amount of the thermal energy supplied to the V-MEMD unit to produce one cubic meter of distillate water, and it is defined as follows:

$$\mathrm{STEC} = \frac{Q^0_h}{v^0_d} \tag{7}$$

The variations in SEEC with inlet heating (evaporator) temperature are depicted in Fig. 11a. The SEEC for the overall system exponentially decreases with increasing inlet heating (evaporator) temperature. Notably, the percent reduction in SEEC for the overall system varies between 75.7% and 81.2% for $T_{h,\mathrm{in}}$ in the range of 55°C–75°C based on different modes, while the percent reduction in SEEC for the V-MEMD unit is 82%–86.7%. The effect of the preheat mode on SEEC is almost negligible, as the electrical-energy consumption for both the modes is the same. In addition, SEEC increases almost linearly with different slopes with increasing cold-side absolute pressure (Fig. 11b), especially at the direct mode and high cold-side absolute pressure P_v of approximately 246.1 mbar. The corresponding SEEC for the overall system is 260.9 kWh/m³. For the V-MEMD unit, SEEC is 44.3 kWh/m³. Using the preheat mode, the SEEC for the overall system was reduced to 180.6 kWh/m³, and that for the V-MEMD unit was reduced to 19 kWh/m³, as depicted in Fig. 11b. As depicted in Fig. 12a, STEC significantly decreases with increasing inlet heating (evaporator) temperature. The overall percentage reduction in STEC for $T_{h,\mathrm{in}}$ in the range of 55°C–75°C is approximately 71% for the preheat mode and 74.6% for the direct mode. The effect of the preheat mode on STEC is evident, as the percent change between the feed-preheating mode and direct mode can vary between 11.6% and 27.7% over the entire temperature range. STEC increases almost linearly with different slopes with increasing cold-side absolute pressure (Fig. 12b), especially at the direct mode and high cold-side absolute pressure P_v of approximately 246.1 mbar. The corresponding STEC is 495.2 kWh/m³. At the preheat mode, STEC was reduced to 311.7 kWh/m³, as depicted in Fig. 12b; this reduction was expected because the pressure drop between the pressure of the feed flow and cold-side absolute pressure inside the multi-effect chambers was reduced. Consequently, the distillate-water production also decreased. The impact of the preheat mode (i.e., feed temperatures) on STEC and SEEC for both the overall system and V-MEMD unit is considerable over the entire range of the cold-side absolute pressure.

As a general conclusion, it can be said that increasing the inlet heating temperature favorably affects the energy consumed. In addition, the electrical energy consumed is important and cannot be ignored while evaluating the energy budget of the solar desalination system. One can consider that the overall specific energies, both electric and thermal, can be 61.8–398.8 and 150.9–674.5 kWh/m³, respectively.
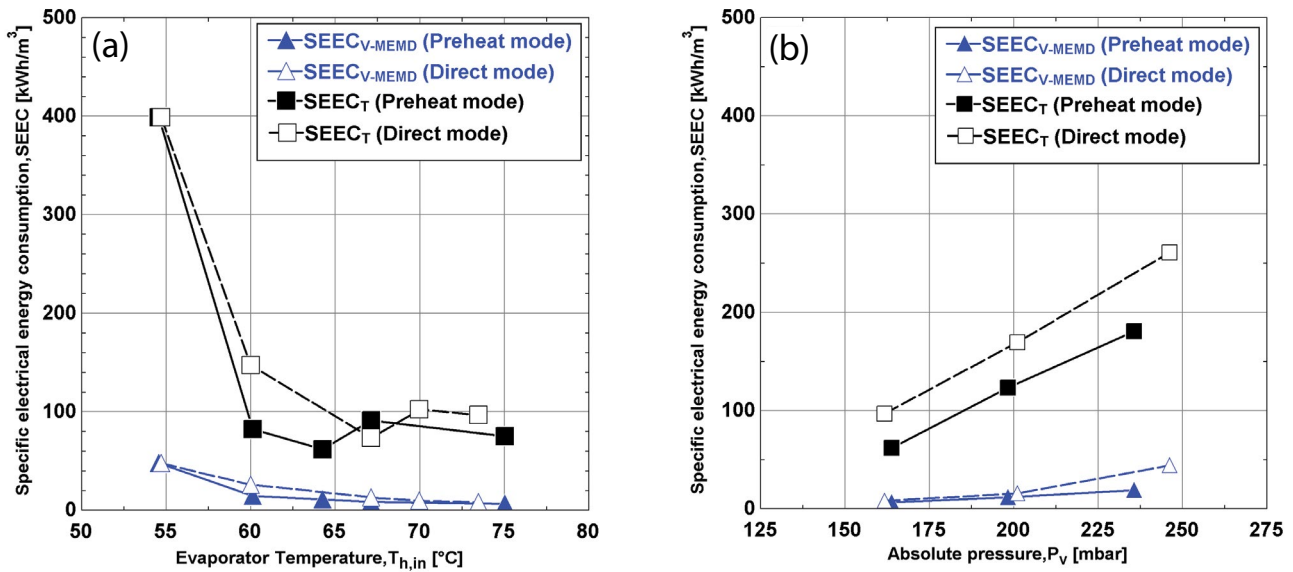
Fig. 11. Variation in SEEC with respect to the (a) inlet evaporator temperature and (b) cold-side absolute pressure, for different feed modes, that is, feed temperatures (v_h^0 = 840 L/h; v_c^0 = 405.5 L/h; $T_{c,in}$ = 25°C–30°C, v_f^0 = 87 L/h; S_f = 1,260 ppm).
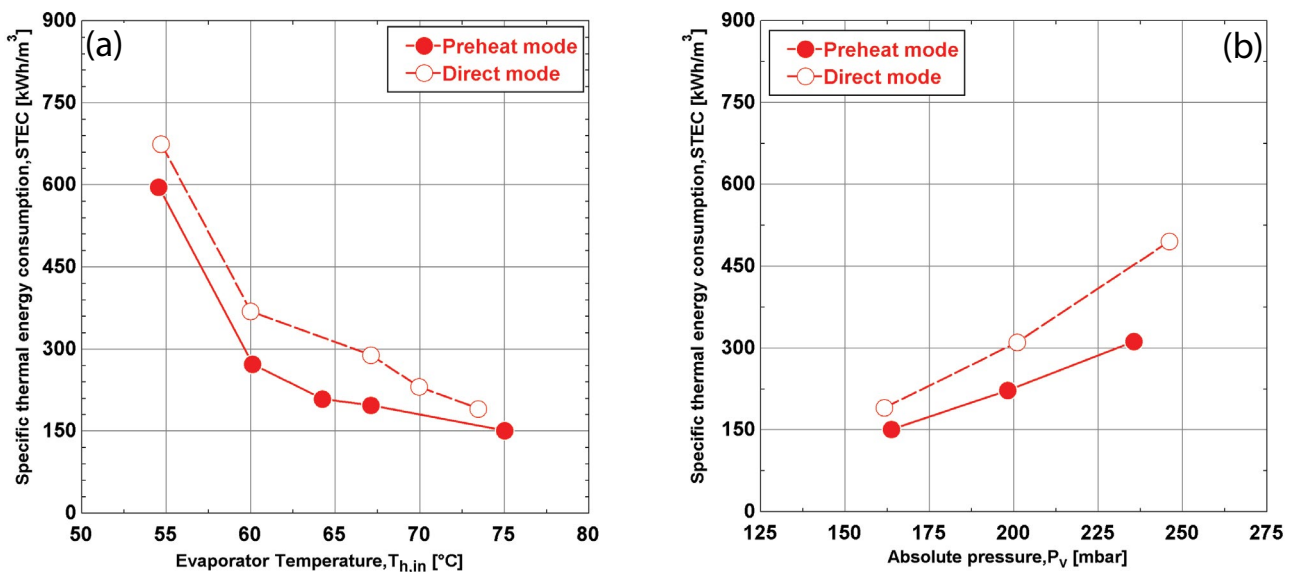
Fig. 12. Variation in STEC with respect to the (a) inlet evaporator temperature and (b) cold-side absolute pressure, for different feed modes, that is, feed temperatures (v_h^0 = 840 L/h; v_c^0 = 405.5 L/h; $T_{c,in}$ = 25°C–30°C; v_f^0 = 87 L/h; S_f = 1,260 ppm).

In addition, we compared the present results with those given in [21,23,25,26]. The operating conditions for all the previous works were considerably close to that for our investigation. The effective membrane area was almost equal, except for Ong et al. [21], whose was approximately 15.2 m². Table 4 presents a comparison of the results of other studies with the present results. The range of water output, permeate flux, and recovery ratio of our investigation are in good agreement with that of the previous work. In addition, the reported GOR and STEC engulf our findings, except that of Ong et al. [21], as the latter reported the

highest values for GOR and STEC. As mentioned earlier, SEEC can be individually defined for the V-MEMD unit and collectively for the overall system. Our range of SEEC for the V-MEMD unit agrees with that of both Zaragoza et al. [23] and Andrés-Mañas et al. [26]. Notably, the latter reported their SEEC values only for the individual V-MEMD unit. Conversely, Ong et al. [21], reported the overall SEEC, which is covered in our investigation as well. Notably, our mass flux and, hence, all mass-flux-dependent parameters such as production rate, recovery rate, and GOR may initiate from zero value, as we tested the system at high values of

Table 4
Comparison of the present results with those obtained from previous works [21, 23, 25, 27]

Reference number	Ong et al. [21]	Zaragoza et al. [23]	Boutikos et al. [25]	Andrés-Mañas et al. [27]	This study
Membrane area (m²)	15.2	5.76	6.3	6.4	5.12
Feed-water type	Saline water and brackish water	Seawater and brackish water	Tap water and saline water	Seawater	Brackish water
Hot water temperature (°C)	Approximately 75–80	85	50–90	60–80	55–75
Feed-flow rate (L/min)	1.9–5.6	Approximately 1.17	1–1.33	1.5–3	1.45–2.32
Feed-water type	Saline and brackish water	Seawater and brackish water	Tap water and saline water	Seawater	Brackish water
Distillate conductivity (μS/cm)	N/A[a]	4–6	N/A[a]	Approximately 3–35	<10
Water output (L/h)	125	N/A[a]	10–32	Approximately 15–55[b]	0–31.8
Permeate flux (kg/m² h)	16.4[b]	Approximately 14[b]	3.2–10.2[b]	2.4–8.5	0–12.24
Recovery ratio (%)	Approximately 39–47	58–59	12.5–40	8.5–40.3	0–36.8
GOR [–]	Approximately 3.8–4.3	N/A[a]	2.46–2.63	1.7–3.2	0–4.24
Specific electrical-energy consumption (kWh/m³)	70.2[b]	18–20	N/A	5–20	61.8–398.8 (overall system)
					6.3–47.6 (V-MEMD unit)
Specific thermal-energy consumption (kWh/m³)	Approximately 128.1[b]	200–400	252–273.8	200–207.7	150.9–674.5

[a]N/A: Not available
[b]Values calculated using the reported data

the cold-side absolute pressure at which water production cannot be achieved, as discussed earlier.

4. Conclusion

Solar-driven multi-effects of the VMD system were described and studied in this study. Experiments were performed in Riyadh city in 6 months (i.e., June, February, March, and April when the daylight is the longest and November and December when the daylight is shortest) over two extreme seasons (i.e., summer and winter). The effects of various design parameters on the performance of the V-MEMD unit were investigated. Summertime had a positive effect on system performance. For example, the startup time, that is, the time required to reach the maximum stable temperature of the thermal storage tank, was 4 h in June, February, March, and April and 5–5.5 h in November and December. Moreover, the maximum distillate-water production was approximately 31.8 L/h, and the corresponding minimum SEEC was 74.9 kWh/m^3 for the overall system and 6.3 kWh/m^3 for the V-MEMD unit. The aforementioned extreme values were obtained for June, March, and April when the feed-preheat mode was enabled.

Real brackish water with the salt concentration of approximately 1,260 ppm (1.260 g/kg) was used as feed the V-MEMD unit. The maximum mass flux of 12.2 kg/m^2 h was obtained. The inlet heating (evaporator) temperature and cold-side absolute pressure were the main parameters influencing the mass flux. Particularly, the inlet heating (evaporator) temperature greater than 55°C, cold-side absolute pressure lower than 200 mbar, and preheat mode promoted high water flux. The best results were produced for the following conditions: preheat mode, $T_{h,\text{in}}$ = 75.03°C, and P_v = 163.7 mbar, and the corresponding recovery ratio reached 36.8%. The GOR obtained at this condition was 4.25, which compares favorably with other reported values. However, we also detailed the SEEC results for the main sub-components of the solar desalination system. It is evident that for performing an accurate evaluation of the energy efficiency of the MD process, we must consider not only the thermal-energy consumption but also the electrical-energy consumption.

Acknowledgments

Symbols

A	—	Hydrophobic membrane area, m^2
E^0	—	Electric energy, W
GOR	—	Gain output ratio
h_{fg}	—	Latent heat, J/kg
$h_{h,\text{out}}$	—	Outlet heating enthalpy, J/kg
$h_{h,\text{in}}$	—	Inlet heating enthalpy, J/kg
$I_{\text{ave}}, I_{\text{max}}$	—	Global irradiation, W/m^2
J	—	Mass flux, kg/m^{2}h
m_d^0	—	Distillate mass flow rate, kg/s
m_h^0	—	Heating mass flow rate, kg/s
P_a	—	Atmospheric pressure, mbar
$P_{h,\text{in}}$	—	Pressure of inlet heating (evaporator), mbar
$P_{h,\text{out}}$	—	Pressure of outlet heating (evaporator), mbar
P_{vf}	—	Vapor pressure of feed, mbar
P_v	—	Cold-side absolute pressure, mbar
Q_{ave}	—	Average solar thermal power, W
Q_h^0	—	Thermal power of evaporator stream in, W
Q_{max}	—	Maximum solar thermal power, W
R	—	Recovery ratio, %
S_f	—	Feed salinity, ppm
SEEC$_{v-\text{MEMD}}$	—	Specific electrical-energy consumption for the V-MEMD unit, kWh/m^3
SEEC$_T$	—	Specific electrical-energy consumption for the overall system, kWh/m^3
STEC	—	Specific thermal-energy consumption, kWh/m^3
T	—	Temperature, °C
T_d	—	Distillate temperature, °C
$T_{h,\text{in}}$	—	Inlet heating (evaporator), °C
$T_{h,\text{out}}$	—	Outlet heating (evaporator), °C
$T_{c,\text{in}}$	—	Inlet cooling (condenser), °C
T_{tank}	—	Thermal storage tank temperature, °C
t	—	Time
v^0	—	Volume flow rate, L/h
v_d^0	—	Distillate flow rate, L/h
v_h^0	—	Heating stream flow rate, L/h
v_f^0	—	Feed-flow rate, L/h
v_c^0	—	Condenser flow rate, L/h

Greek

ρ	—	Density

Subscript

c	—	Cooling stream
d	—	Distillate water
f	—	Feed stream
h	—	Heating stream
R	—	Refrigerating system
S	—	Solar system

References

[1] M.K. Wittholz, B.K. O'Neill, C.B. Colby, D. Lewis, Estimating the cost of desalination plants using a cost database, Desalination, 229 (2008) 10–20.
[2] S.A. Kalogirou, Seawater desalination using renewable energy sources, Prog. Energy Combust. Sci., 31 (2005) 242–281.
[3] E. Tzen, D. Theofilloyianakos, M. Sigalas, K. Karamanis, Design and development of a hybrid autonomous system for seawater desalination, Desalination, 166 (2004) 267–274.
[4] H. Chang, G.-B. Wang, Y.-H. Chen, C.-C. Li, C.-L. Chang, Modeling and optimization of a solar driven membrane distillation desalination system, Renewable Energy, 35 (2010) 2714–2722.
[5] M. Thomson, D. Infield, Laboratory demonstration of a photovoltaic-powered seawater reverse-osmosis system without batteries, Desalination, 183 (2005) 105–111.

[6] V.G. Gude, N. Nirmalakhandan, S. Deng, Renewable and sustainable approaches for desalination, Renewable Sustainable Energy Rev., 14 (2010) 2641–2654.

[7] J. Blanco, S. Malato, P. Fernández-Ibañez, D. Alarcón, W. Gernjak, M. Maldonado, Review of feasible solar energy applications to water processes, Renewable Sustainable Energy Rev., 13 (2009) 1437–1445.

[8] F. Banat, N. Jwaied, M. Rommel, J. Koschikowski, M. Wieghaus, Desalination by a "compact SMADES" autonomous solar powered membrane distillation unit, Desalination, 217 (2007) 29–37.

[9] M.R. Qtaishat, F. Banat, Desalination by solar powered membrane distillation systems, Desalination, 308 (2013) 186–197.

[10] G. Meindersma, C. Guijt, A. De Haan, Desalination and water recycling by air gap membrane distillation, Desalination, 187 (2006) 291–301.

[11] J.-P. Mericq, S. Laborie, C. Cabassud, Vacuum membrane distillation of seawater reverse osmosis brines, Water Res., 44 (2010) 5260–5273.

[12] Y.-H. Chen, Y.-W. Li, H. Chang, Optimal design and control of solar driven air gap membrane distillation desalination systems, Appl. Energy, 100 (2012) 193–204.

[13] H.E. Fath, S.M. Elsherbiny, A.A. Hassan, M. Rommel, M. Wieghaus, J. Koschikowski, M. Vatansever, PV and thermally driven small-scale, stand-alone solar desalination systems with very low maintenance needs, Desalination, 225 (2008) 58–69.

[14] J. Koschikowski, M. Wieghaus, M. Rommel, V.S. Ortin, B.P. Suarez, J.R.B. Rodríguez, Experimental investigations on solar driven stand-alone membrane distillation systems for remote areas, Desalination, 248 (2009) 125–131.

[15] E. Guillén-Burrieza, J. Blanco, G. Zaragoza, D.-C. Alarcón, P. Palenzuela, M. Ibarra, W. Gernjak, Experimental analysis of an air gap membrane distillation solar desalination pilot system, J. Membr. Sci., 379 (2011) 386–396.

[16] S.T. Bouguecha, S.E. Aly, M.H. Al-Beirutty, M.M. Hamdi, A. Boubakri, Solar driven DCMD: performance evaluation and thermal energy efficiency, Chem. Eng. Res. Des., 100 (2015) 331–340.

[17] J.-G. Lee, W.-S. Kim, J.-S. Choi, N. Ghaffour, Y.-D. Kim, Dynamic solar-powered multi-stage direct contact membrane distillation system: concept design, modeling and simulation, Desalination, 435 (2018) 278–292.

[18] R. Schwantes, A. Cipollina, F. Gross, J. Koschikowski, D. Pfeifle, M. Rolletschek, V. Subiela, Membrane distillation: solar and waste heat driven demonstration plants for desalination, Desalination, 323 (2013) 93–106.

[19] H.W. Chung, J. Swaminathan, D.M. Warsinger, Multistage vacuum membrane distillation (MSVMD) systems for high salinity applications, J. Membr. Sci., 497 (2016) 128–141.

[20] M. Khayet, Solar desalination by membrane distillation: dispersion in energy consumption analysis and water production costs (a review), Desalination, 308 (2013) 89–101.

[21] C.L. Ong, W. Escher, S. Paredes, A. Khalil, B. Michel, A novel concept of energy reuse from high concentration photovoltaic thermal (HCPVT) system for desalination, Desalination, 295 (2012) 70–81.

[22] K. Zhao, W. Heinzl, M. Wenzel, S. Büttner, F. Bollen, G. Lange, S. Heinzl, N. Sarda, Experimental study of the memsys vacuum-multi-effect-membrane-distillation (V-MEMD) module, Desalination, 323 (2013) 150–160.

[23] G. Zaragoza, A. Ruiz-Aguirre, E. Guillén-Burrieza, Efficiency in the use of solar thermal energy of small membrane desalination systems for decentralized water production, Appl. Energy, 130 (2014) 491–499.

[24] E.S. Mohamed, P. Boutikos, E. Mathioulakis, V. Belessiotis, Experimental evaluation of the performance and energy efficiency of a vacuum multi-effect membrane distillation system, Desalination, 408 (2017) 70–80.

[25] P. Boutikos, E.S. Mohamed, E. Mathioulakis, V. Belessiotis, A theoretical approach of a vacuum multi-effect membrane distillation system, Desalination, 422 (2017) 25–41.

[26] J. Andrés-Mañas, L. Roca, A. Ruiz-Aguirre, F. Acién, J.D. Gil, G. Zaragoza, Application of solar energy to seawater desalination in a pilot system based on vacuum multi-effect membrane distillation, Appl. Energy, 258 (2020) 114068.

[27] J. Andrés-Mañas, A. Ruiz-Aguirre, F. Acién, G. Zaragoza, Assessment of a pilot system for seawater desalination based on vacuum multi-effect membrane distillation with enhanced heat recovery, Desalination, 443 (2018) 110–121.

[28] A. Chafidz, S. Al-Zahrani, M.N. Al-Otaibi, C.F. Hoong, T.F. Lai, M. Prabu, Portable and integrated solar-driven desalination system using membrane distillation for arid remote areas in Saudi Arabia, Desalination, 345 (2014) 36–49.

[29] Y. Wang, Z. Xu, N. Lior, H. Zeng, An experimental study of solar thermal vacuum membrane distillation desalination, Desal. Water Treat., 53 (2015) 887–897.

[30] A. Luo, N. Lior, Critical review of membrane distillation performance criteria, Desal. Water Treat., 57 (2016) 20093–20140.

Supplementary information

Additional experimental results
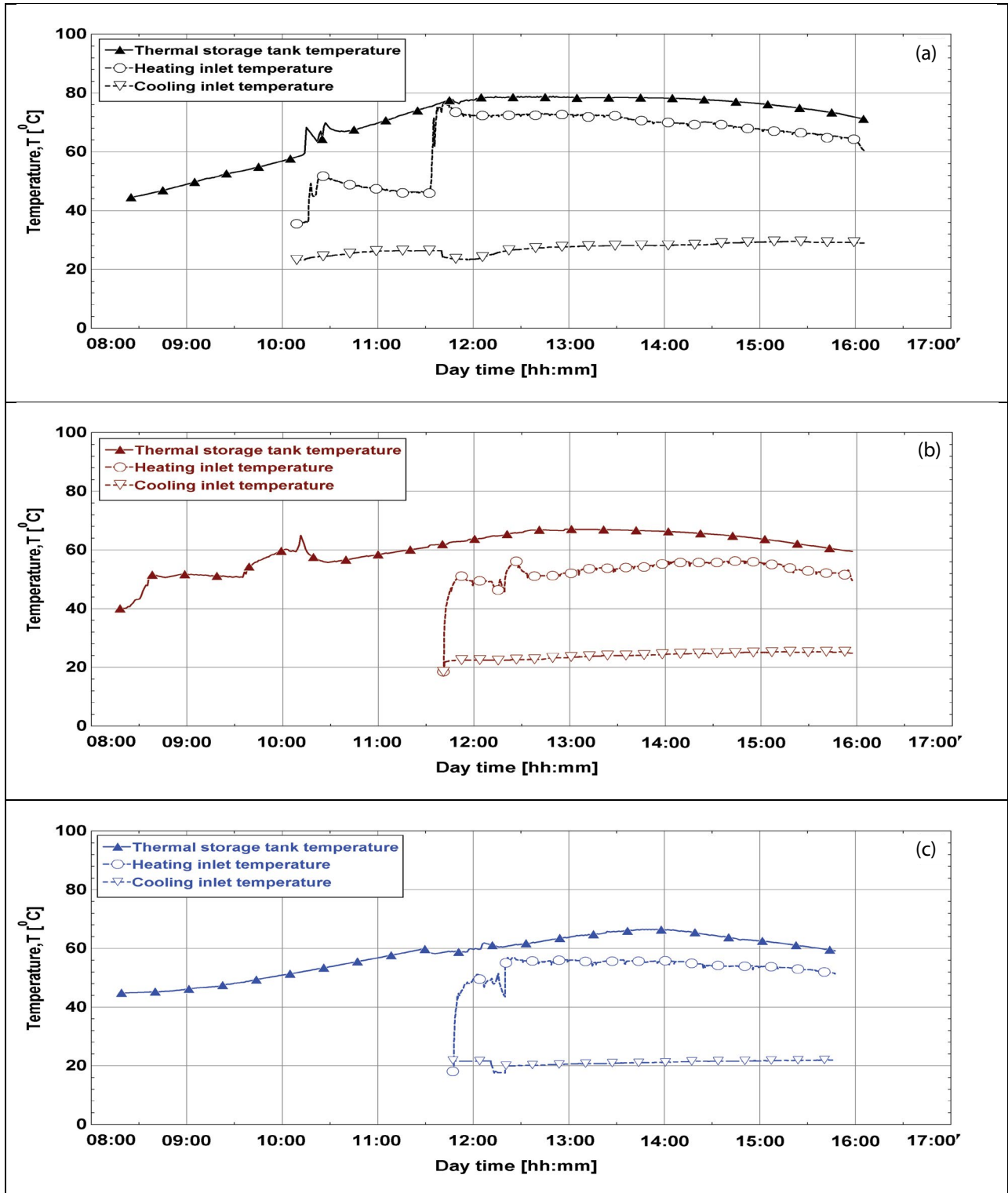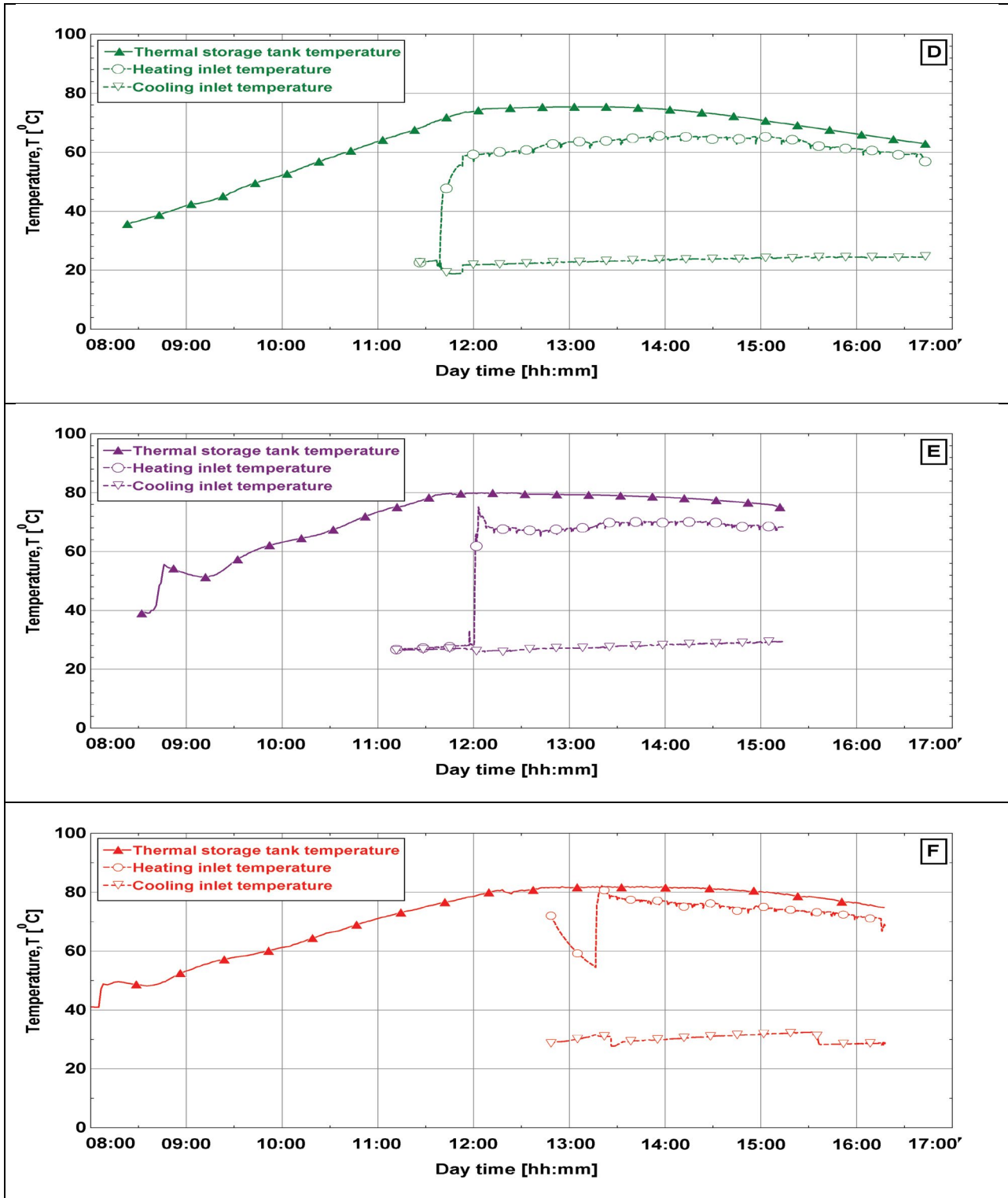
Fig. S1. Measured hourly thermal storage tank, inlet heating, and inlet cooling temperatures during the tests; (8 AM–4 PM) at KSU for different typical days in specified months ((a) June, (b) November, (c) December, 2017 and (d) February, (e) March, and (f) April, 2018).

Cleaning method

The cleaning method has two necessary steps, as shown as follows:

- The first step is called the pretreatment of the test water flowing to the feed tank. Which is continuously treated by an ultrafiltration cartridge (it is made of hollow fiber).
- The last step is called flushing; there are several procedures involved in this step that is summarized as follows:
    - Switch off all filling process on the heating and cooling circuit.
    - Check all valves and brine hose to the correct position.
    - Switch on the V-MEMD unit, but do not operate the vacuum pump.
    - The thermal source is not enabled.
    - Isolated from the heat pump (refrigerating) system, the feed stream is allowed to enter directly into the V-MEMD unit, as described in Fig. 2.
    - Gradually raise the flow of the feed stream to reach higher than 150 L/h. It is important not to recycle the feed stream again.
    - Repeat the flushing process several times depending on the degree of contamination.